Temperature–RH Dependent Viscosity of Organic Aerosols from 273 to 303 K: Implications for Global N$_2$O$_5$ Uptake

Atta Ullah[1], Ying Li[2], Mijung Song[1,3]

[1]Department of Earth and Environmental Sciences, and Earth Environmental System Research Center, Jeonbuk National University, Jeollabuk-do Jeonju-si 54896, Republic of Korea; [2] Key Laboratory of Industrial Ecology and Environmental Engineering (Ministry of Education), School of Environmental Science and Technology, Dalian University of Technology, Dalian 116024, China; [3]Department of Environment and Energy, Jeonbuk National University, Jeollabuk-do Jeonju-si 54896, Republic of Korea

*Corresponding author: Mijung.Song@jbnu.ac.kr

Summary: 21 pages, 11 figures, 1 table

S1. Flow-cell calibration and particle conditioning time determination

In both bead-mobility and poke-and-flow experiments, the flow-cell was calibrated for relative humidity (RH) using the deliquescence points of three salts including K_2CO_3, NaCl, and $(NH_4)_2SO_4$ (Winston and Bates, 1960). The experimentally determined deliquescence RH at each measurement temperature 273, 283, 293, and 303 K were compared with literature. The RH accuracy was within ± 2.0 % and the temperature was controlled within ± 1 K of the target.

Prior to each experiment, particles deposited on a hydrophobic substrate were conditioned at the target RH of the carrier gas to allow sufficient equilibration with the surrounding gases. Conditioning times were adjusted depending on the experimental temperature and technique. To evaluate whether the samples reached near-equilibrium with the target RH, we applied a method previously reported in the literature (Kiland et al., 2023a; Smith et al., 2021a; Kiland et al., 2023b; Maclean et al., 2021; Evoy et al., 2021; Smith et al., 2021b). This method involves comparing experimental conditioning time to the characteristic mixing time of water within organic aerosol (OA), $\tau_{mix,H2O}$, calculated:

$$\tau_{mix,H2O} = \frac{d_p^2}{4\pi^2 D_{H2O}(T, RH)} \tag{S1.1}$$

Here, d_p represents the particle diameter. $D_{H_2O}(T, RH)$ is the RH- and temperature-dependent diffusion coefficient of water in OA. The value of D_{H_2O} was calculated using the fractional Stokes–Einstein equation, which accounts for the link between viscosity and diffusion in cases where the diffusing species are comparable in size to, or smaller than, the molecules forming the molecules (Evoy, 2020):

$$D_{H2O}(T, RH) = D°_{H2O}(T) \times \left(\frac{\eta°_{H2O}(T)}{\eta(T, RH)}\right)^{\xi} \tag{S1.2}$$

In this equation, $D°_{H2O}(T)$ is the the self-diffusion of water calculated with the Stokes-Einstein equation at 293 K (2.15×10^{-9} m^2 s^{-1}). $\eta°_{H2O}(T)$ is the viscosity of pure water obtained from literature with values of 1.78×10^{-3} Pa·s at 273 K, 1.31×10^{-3} Pa·s at 283 K, 1×10^{-3} Pa·s at 293K, and 8.14×10^{-4} Pa·s at 303 K.(Weight, 2019). $\eta(T, RH)$ is the measured viscosity of sucrose at the corresponding RH and temperature. ξ is the fractional exponent, using Eq. (S1.3), which accounts for the relative size of the diffusing molecule and the matrix:

$$\xi = 1 - \left[A \times \exp\left(-B\frac{r_{diff}}{r_{matrix}}\right)\right] \tag{S1.3}$$

where coefficient values of A = 0.73 and B = 1.79 (Evoy et al., 2020), r_{diff} hydrodynamic radius of water of 0.1 nm.(Price et al., 2016) The matrix radius, r_{matrix}, of the sucrose molecule was calculated under the assumption of spherical geometry, using 342.30 g mol^{-1} and a density of 1.67 g cm^{-3}(Haynes, 2016), resulting in r_{matrix} = 0.44 nm and ξ = 0.51. Conditioning durations for the other temperatures (273, 283, 293 and 303 K) are summarized in Table S1.

40 In addition to water, we also estimated the mixing times of organic molecules ($\tau_{mix,org}$) to assess potential diffusion
41 limitations within the particle matrix itself. This is particularly relevant under conditions where semi-solid or glassy
42 states may impede equilibration. The diffusion coefficient of organics (D_{org}) was calculated using the classical
43 Stokes–Einstein equation (Eq. S1.4):(Evoy et al., 2019; Evoy et al., 2020)

$$D_{org}(T, RH) = \frac{kT}{6\pi\eta_{org}(RH, T)R_{diff}} \qquad (S1.4)$$

44 where k is the Boltzmann constant, η_{org} is the temperature-and-RH dependent viscosity of OA, and R_{diff} is the
45 radius of the diffusing molecules. We used 0.4 nm for R_{diff}, consistent with typical organic molecules of similar
46 molecular weight and density. Using the estimated diffusion coefficients, the mixing time of organics was
47 calculated as:

$$\tau_{mix,org} = \frac{d_p{}^2}{4\pi^2 D_{org}(T, RH)} \qquad (S1.5)$$

48
49 A particle diameter of 200 nm was used in all calculations, consistent with the typical size of secondary organic
50 aerosol (SOA) particles observed in the atmosphere (Riipinen et al., 2011; Pöschl et al., 2010). The $\tau_{mix,org}$ value
51 represents the time required for the concentration of the diffusing species at the particle's center to attain 1/e of the
52 equilibrium concentration.

53 The diffusivity coefficient of N_2O_5 in OA (D_{N2O5}), which is needed in calculations of N_2O_5 uptake coefficient, is
54 also determined using the fractional Stokes-Einstein equation (S1.2 and S1.3). In Eq. S1.3, the hydrodynamic radius
55 of N_2O_5 is set to be 0.25 nm (Grzinic et al., 2015).

S2. Viscosity parameterization of sucrose-H_2O droplets

We parameterized the viscosity of sucrose-H_2O droplets as a function of RH and temperature, following the approach proposed by Kiland et al. (2023) Experimental data at 293 ± 1 K was fitted using a mole-fraction-based Arrhenius mixing rule (Eq. S2.1)

$$\log\big(\eta(\text{RH}, 293\text{K}) = x_{\text{org}} \log_{10}\big(\eta_{\text{org,dry}}\big) + \big(1 - x_{\text{org}}\big)\log(\eta°_{\text{H2O}}\big) \tag{S2.1}$$

where $\eta(\text{RH}, 293\text{K})$ is the viscosity of the mixture at room temperature, $\eta_{org,dry}$ is the viscosity of the organic component at 0% RH (1×10^{12} Pa·s), and $\eta°_{H_2O}$ is the viscosity of pure water (1×10^{-3} Pa·s).

The mole fraction of organic components, x_{org}, was calculated from the mass fraction using:

$$x_{\text{org}} = \frac{\dfrac{w_{\text{org}}}{M_{\text{org}}}}{\dfrac{w_{\text{org}}}{M_{\text{org}}} + \dfrac{1 - w_{\text{org}}}{M_{\text{H}_2\text{O}}}} \tag{S2.2}$$

where w_{org} is the mass fraction of the organic component, and M_{org} and M_{H_2O} are the molecular weights of sucrose and water, respectively. w_{org} was determined from the water activity ($a_w = \text{RH}/100$) using a mass-based hygroscopicity parameter k, as shown in Eq. S2.3.

$$w_{\text{org}} = \left(1 + k\left(\frac{a_w}{1 - a_w}\right)\right)^{-1} \tag{S2.3}$$

To evaluate the tropospheric distribution of predicted sucrose–H_2O droplet phase state and mixing times, we utilized monthly mean reanalysis data for temperature and RH from the Copernicus Climate Data Store (https://cds.climate.copernicus.eu/) (Hersbach et al., 2023). The dataset provides global coverage from 90°N to 90°S and 180°W to 180° E, with temporal resolution spanning January 2020 to December 2024. The altitude (h) corresponding to each pressure level was computed using the following equation derived from the barometric formula:

Fitting the experimental data at 293 K yielded the value of $k = 0.061 \pm 0.0023$. As shown in Figure S8, the model provides a good fit to the experimental data, supporting the robustness of the parameterization. Peters and Kreidenweis (2007) reported k values between 0.01 and 0.5 for diverse organic compounds, highlighting variability in hygroscopicity with molecular structure.

78 **S3. Collection of global ambient zonal-RH and -temperature**
79

$$h = \frac{1 - \left(\frac{P}{P_o}\right)^{\frac{R\lambda}{M_{air}}}}{\lambda/T_o} \qquad (3)$$

80
81 where P is the pressure at the given level (1000 hPa – 100 hPa), p_o is the pressure at sea level (101325 Pa), R is the
82 gas constant (8.314 J mol^{-1} K^{-1}), λ is the temperature lapse rate (6.5 K km^{-1}), M_{air} is the molecular mass of the air
83 (28.97 g mol^{-1}), and T_o is the mean temperature at the surface (288.15 K). To construct latitude–altitude profiles,
84 the monthly RH and temperature values were averaged across all longitudes at each latitude and pressure level.
85

86

87
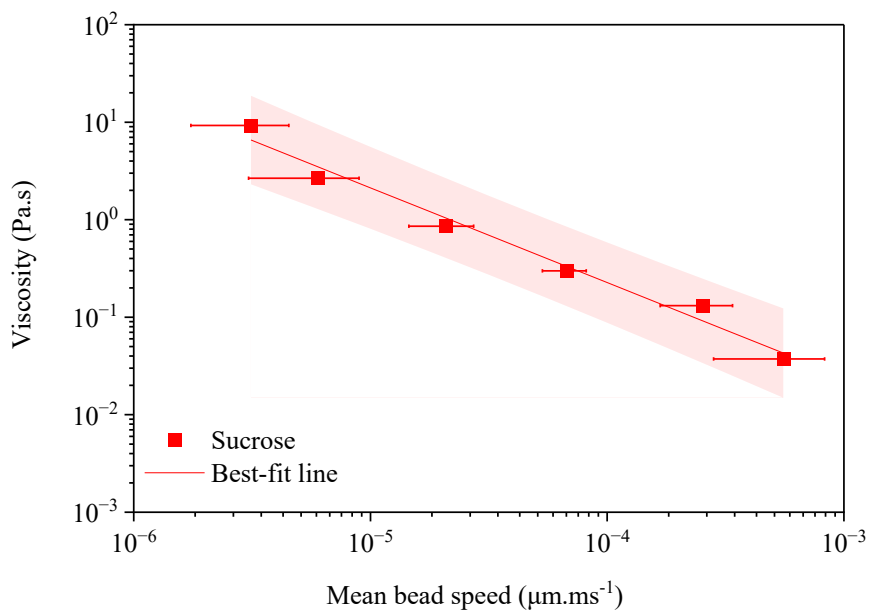
Figure S1: Calibration line illustrating the relationship between mean bead speeds and viscosities of sucrose-H₂O droplets at varying relative humidity (RH) levels. A linear regression, shown by the red dotted line, fits the data with the equation: $viscosity = 0.00003 \times (mean\ bead\ speed)^{-0.971}$**. The pink area denotes 95% prediction bands of fitting to the data in this study. The uncertainty in mean bead speed along** *x*–**axis is calculated from standardization of** $2 - 5$ **beads within** $3 - 5$ **particles for each RH value.**

93

| Temp	Particle position 1	Particle position 2	Particle position 3
273 K, ~80% RH	1292,554 1324,559 1292,588 0 sec	1311,568 1337,571 1306,601 68400 sec	1296,585 1311,567 1281,601 98100sec
283 K, ~80% RH	2297,448 2328,473 2350,472 0 sec	1258,255 1280,270 1267,305 2400 sec	1216,262 1337,281 1228,267 6000 sec
293 K, ~80% RH	1375,119 1390,134 1374,140 0 sec	1361,128 1369,146 1357,146 1200 sec	1356,127 1358,151 1510 sec
303 K, ~73% RH	901, 449 902,469 888,468 0 sec	900,450 901,472 891,471 600 sec	903, 463 897,490 890,489 2280 sec

Figure S2: Optical images of sucrose-H2O droplets during a typical bead-mobility experiment at different temperatures. Three labeled beads with tracked x and y coordinates were used to determine average bead speeds using ImageJ software. The size of the scale bar is 20 μm.
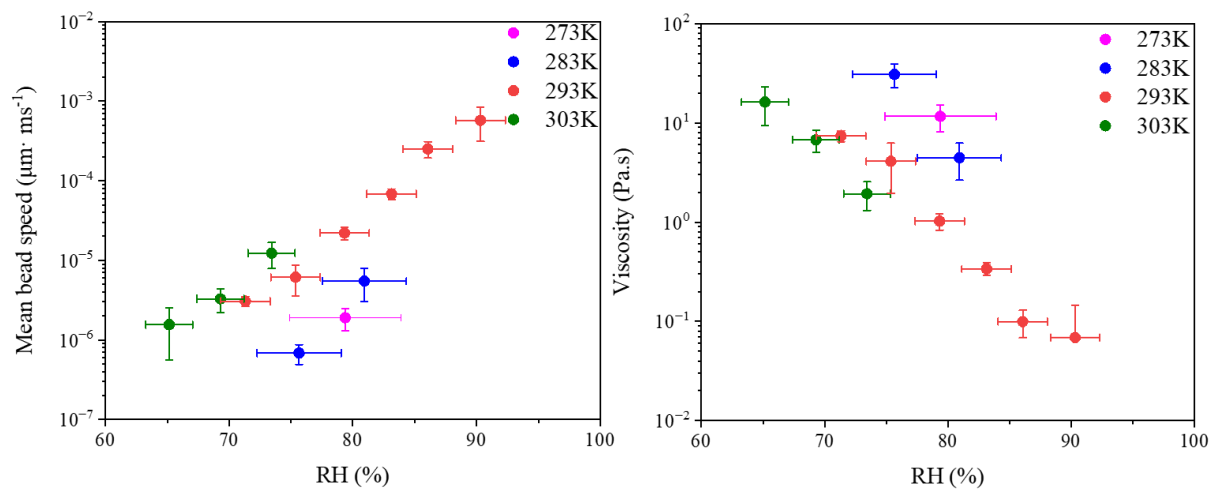
99
100 Figure S3: (a) Mean bead speed and (b) resulted viscosities from bead-mobility experiments for sucrose-H2O droplets
101 as a function of temperature and relative humidity (RH). The x-axis error bars represent the uncertainty in RH from
102 the RH sensor during calibration at each temperature, while y-axis error bars indicate the standard deviation of the
103 measured bead speeds and viscosity calculated from 3 – 5 beads across 2 – 5 particles at each RH level.

104

| Temp	Pre-poking	Poking	Post-poking	$\tau_{exp,flow}$
273K, ~ 50% RH			0 sec	6768 sec
283 K, ~ 50% RH			0 sec	397 sec
293 K, ~ 50% RH			0 sec	25 sec
303 K, ~ 50% RH			0 sec	3 sec
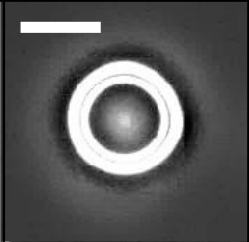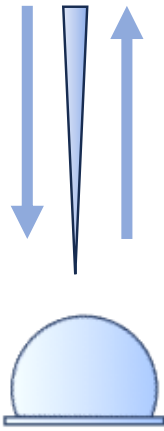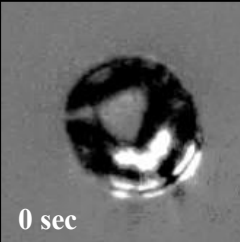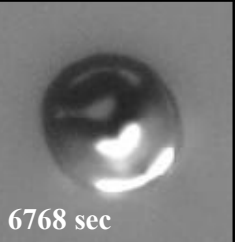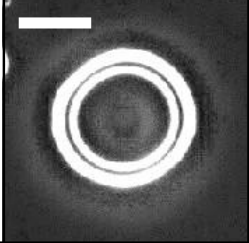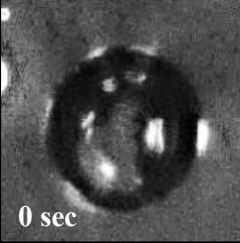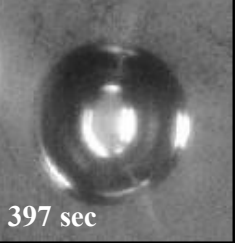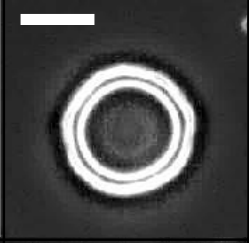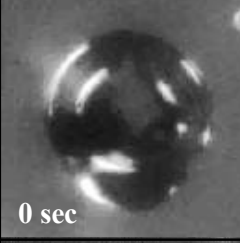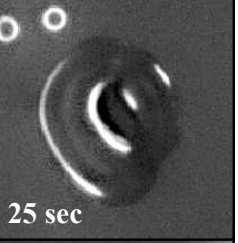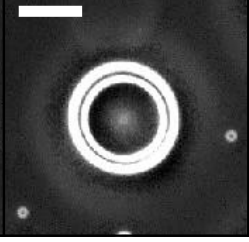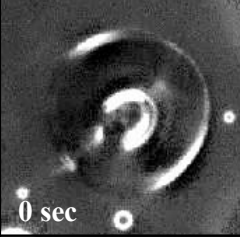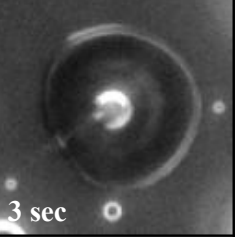
Figure S4: Optical images for experimental flow times (τexp, flow) during poke-and-flow experiments at different temperatures. White scale bar indicates 20 μm.
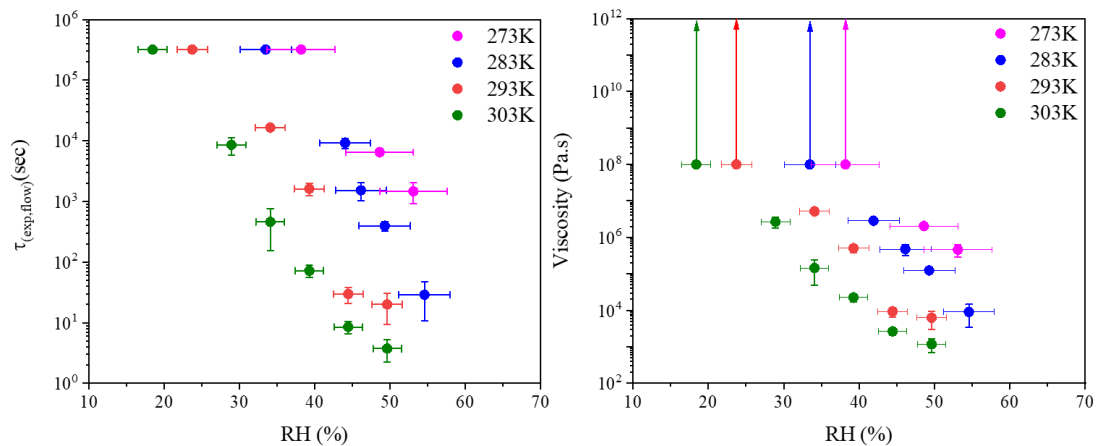
Figure S5: (a) Mean experimental flow time (τ(exp, flow)) from poke-and-flow experiments for sucrose-H2O droplets as a function of temperature and relative humidity (RH). The x-axis error bars represent the uncertainty in RH from the RH sensor during calibration at each temperature, while y-error bars indicate the standard deviation of the measured τ(exp, flow), calculated from measurements of 3 – 4 particles at each RH level. (b) Resulted viscosities from the τ(exp, flow) and the equation proposed by Sellier et al. (2015) The y-error bars indicate the standard deviation of the measured viscosity.

Temp	Pre-poking	Poking	After 0 sec	After 1 hr	After 2 hrs
273K, ~ 38% RH	38% RH				
283K, ~ 33% RH	33% RH				
293K, ~ 24% RH	24% RH				
303K, ~ 18% RH	18% RH				
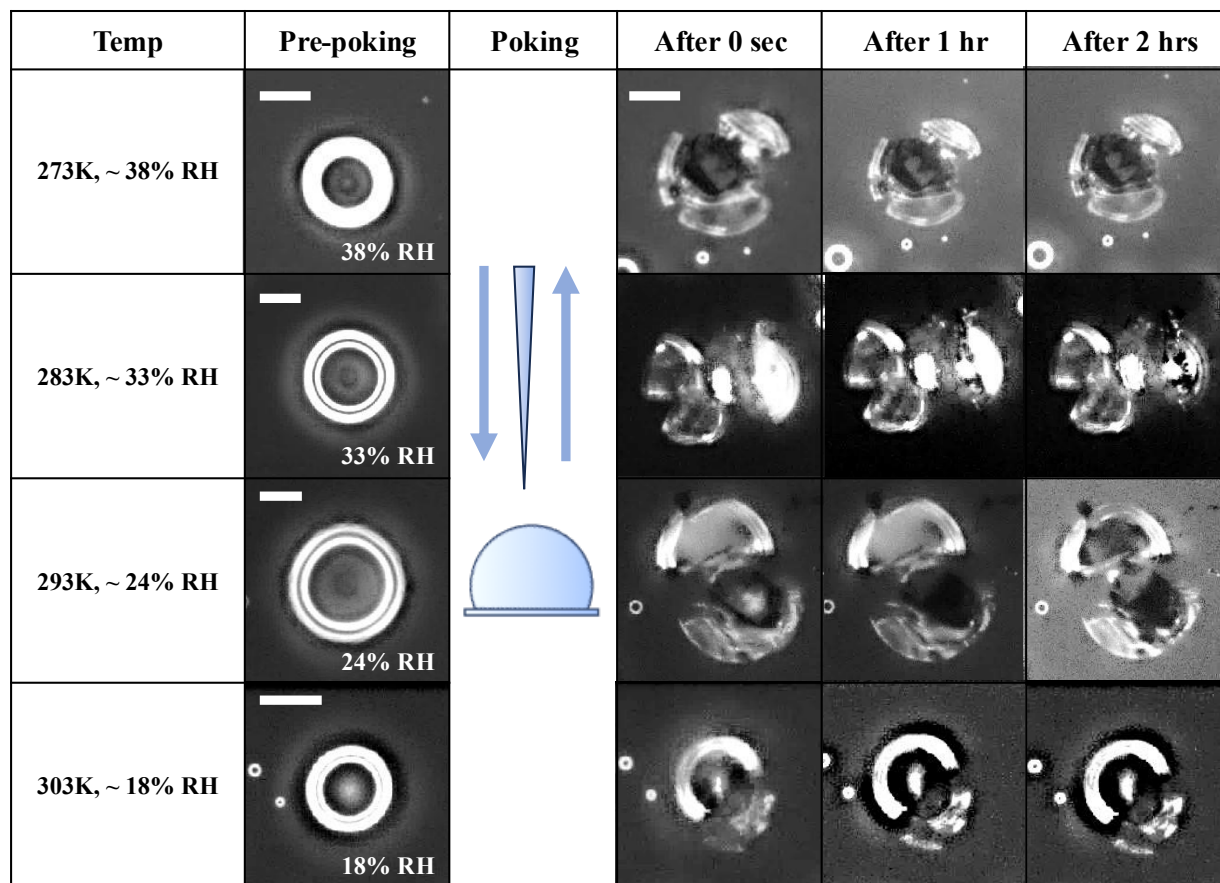
Figure S6: Optical images of sucrose-H2O droplets during poke–and–flow experiments at different temperatures. Observations were made when particles cracked at certain relative humidity (RH), and they were then monitored for longer than 2 hours, with no evidence of flow restoration was detected. RH was consistently regulated throughout the pre-poking, poking, and post-poking stages. White scale bars represent 20 μm.

124
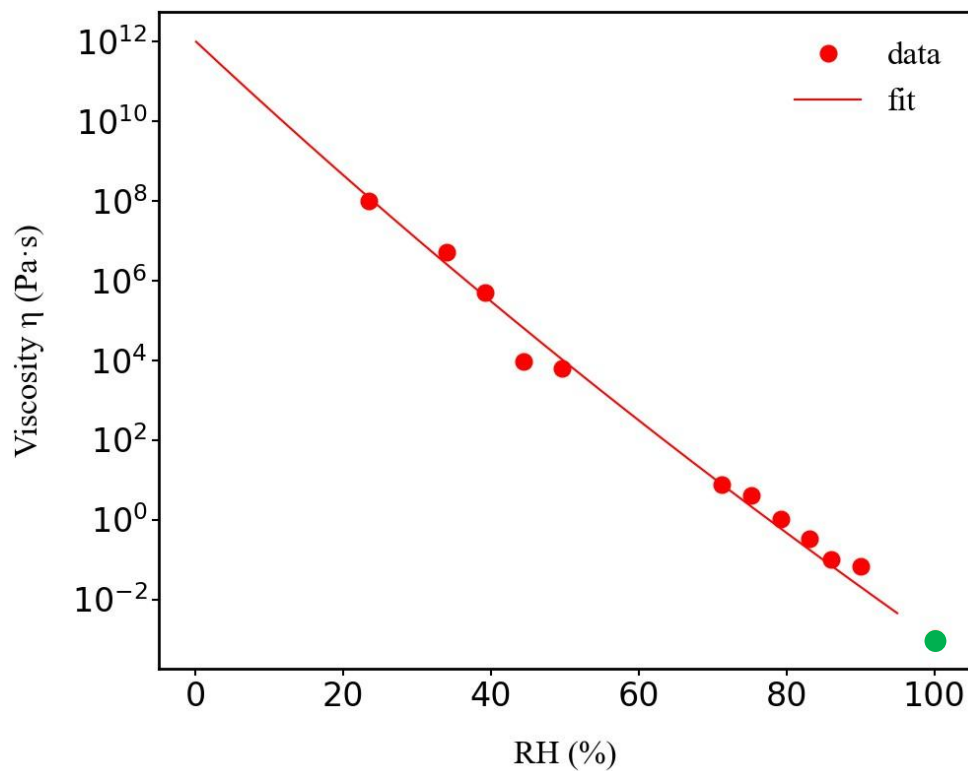
125

126 **Figure S7: The log viscosity of sucrose-H2O droplets as a function of RH at room temperature. The solid line is a mole-**
127 **fraction-based Arrhenius mixing rule fit to the viscosity data (eq S2.1), which yields a hygroscopicity parameter, κ =**
128 **0.061. The point at 100% RH (green circle) represents the viscosity of water at room temperature.**

129

130
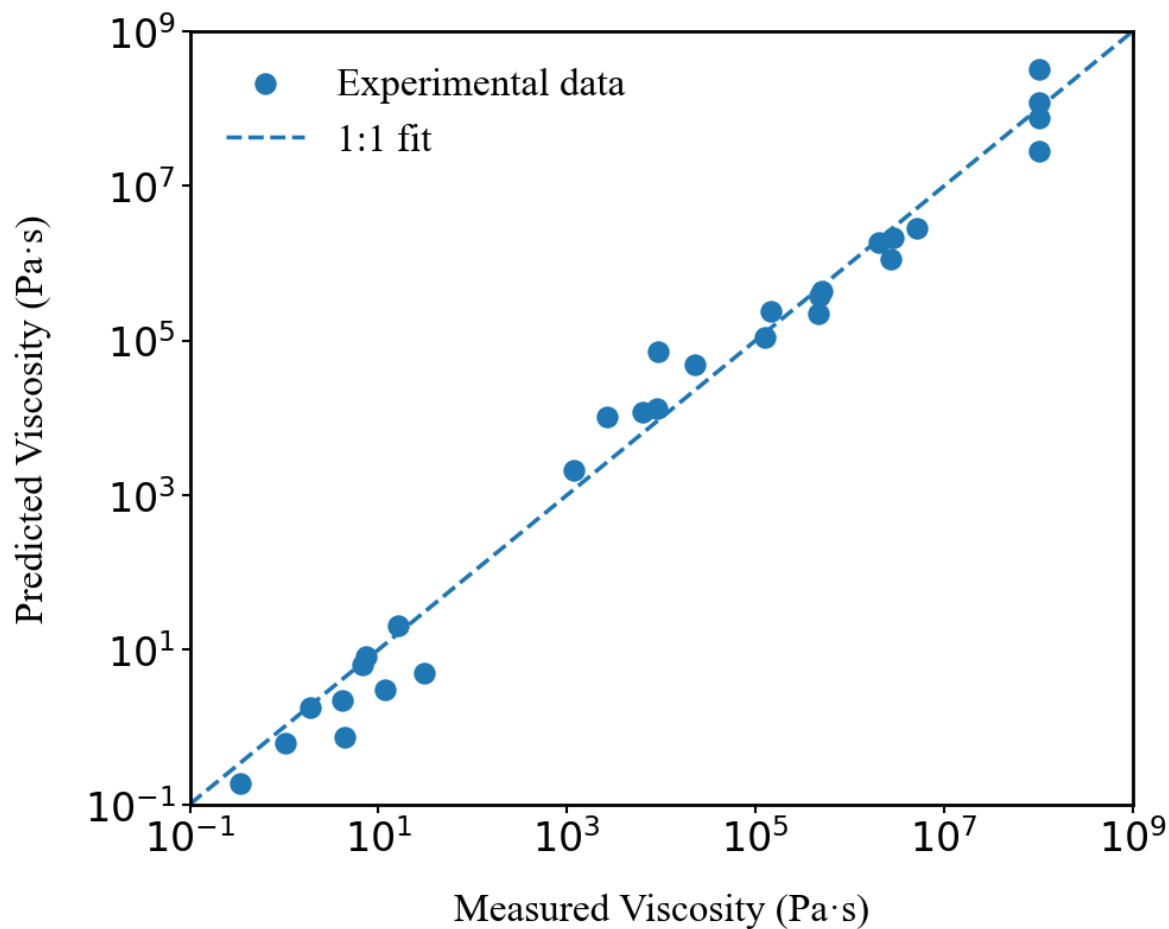
Figure S8: Comparison of experimental and predicted viscosity values for sucrose-H2O droplets. The experimental values (blue circles) were measured between 273 and 303 K and ~20 to ~90 % RH, whereas predicted viscosities (dashed line) were calculated using the VFT equation. The fitting procedure yields the fragility parameter (Df) value of 13 ± 1.

135
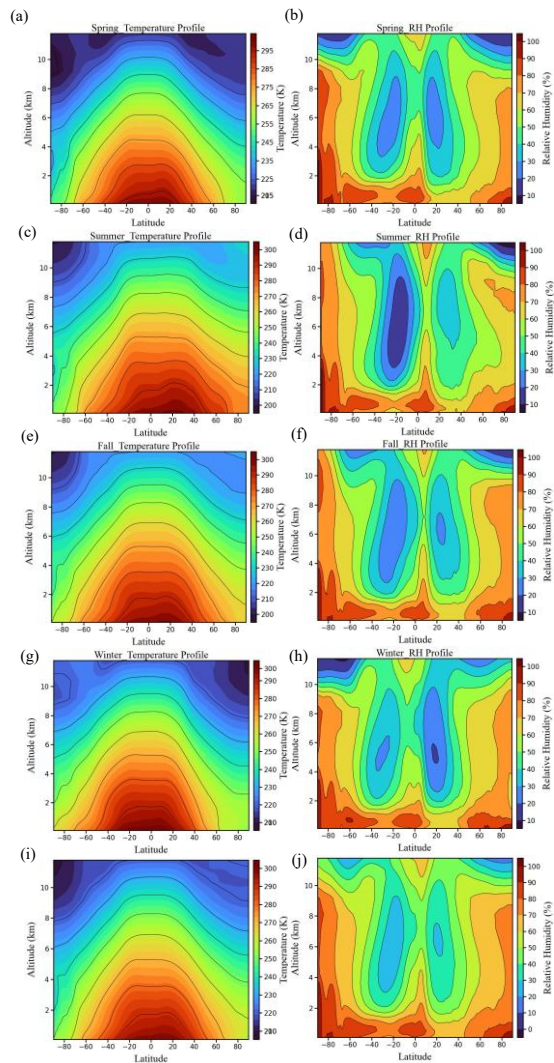
Figure S9: Altitude–latitude profiles of zonal-mean temperature and RH obtained from Copernicus Climate Data Store (https://cds.climate.copernicus.eu/) , averaged seasonally and annually over the period 2020-01-01 to 2024-12-01. Panels present seasonal profiles for spring (a and b), summer (c and d), fall (e and f), and winter (g and h), showing temperature and RH, respectively. Panels (I and j) display the annual average zonal-mean profiles of temperature and RH.

140
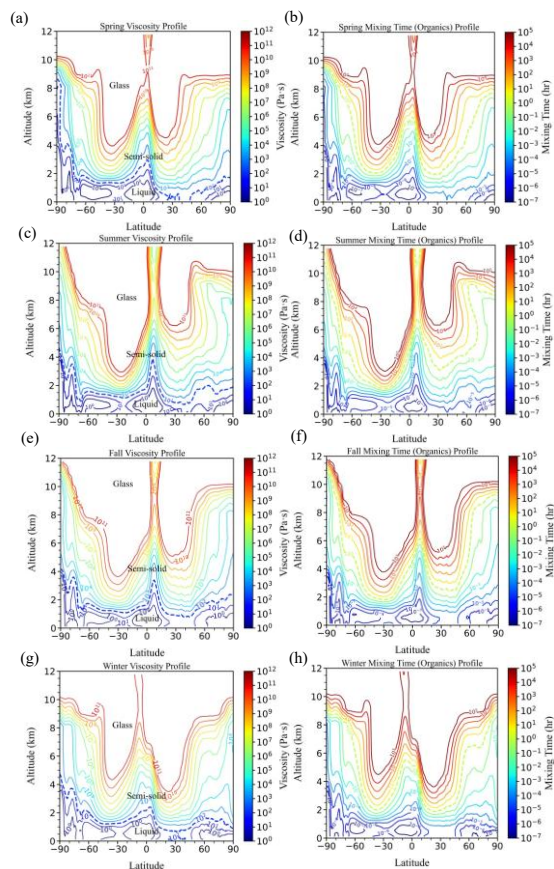
Figure S10: Seasonal zonal-mean profiles of viscosity and mixing time of sucrose droplets as a function of altitude and latitude, derived from temperature and RH data obtained from Copernicus Climate Data Store (https://cds.climate.copernicus.eu/) and averaged over the period 2020-01-01 to 2024-12-01. Panels (a and b) present viscosity and mixing time for spring, panels (c and d) for summer, panels (e and f) for fall, and panels (g and h) for winter. The blue dashed line shows the transition from liquid to semi-solid state. The light green dashed shows the mixing time of 1 hr.
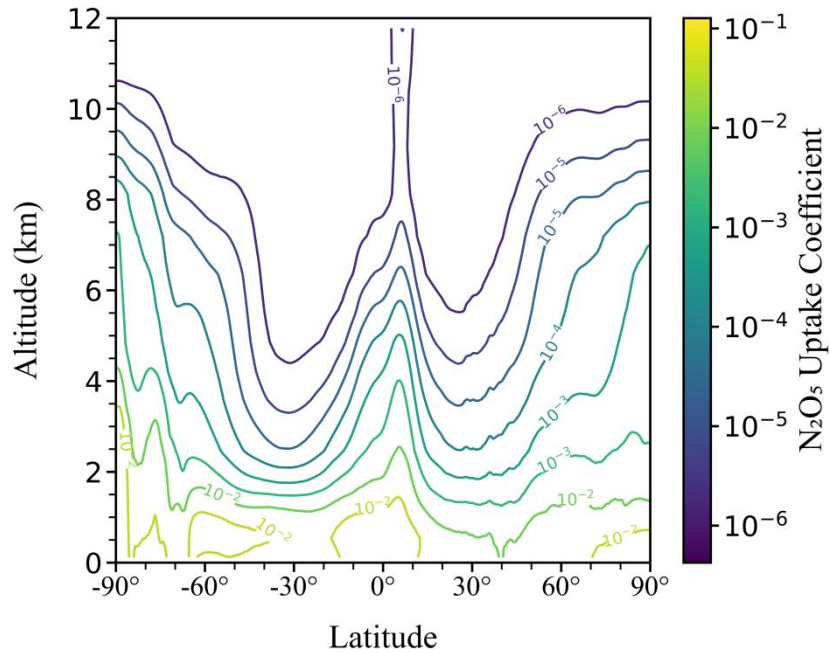
Figure S11: N2O5 uptake coefficient in 200 nm sucrose droplets as a function of altitude and latitude based on annual average zonal-mean RH and temperature fields for the years 2020 to 2024, obtained from Copernicus Climate Data Store (https://cds.climate.copernicus.eu/). Surface hydrolysis is not considered in calculations of N2O5 uptake coefficient (Γ_s is set to be 0 in Eq. 3).

169 **Table S1.** Summary of the conditioning time for sucrose-H_2O droplets at different temperature and RH conditions.
170 τ_{mix,H_2O} values are the calculated characteristic mixing time of water within the sucrose-H_2O droplets based on the
171 calculated diffusion coefficient of water. $\tau_{conditioning}$ values represent the experimental conditioning time. $\tau_{conditioning}$
172 / τ_{mix,H_2O} ratio values exceeding 1 indicates that the particles have likely reached equilibrium with the surrounding
173 RH.
174

RH	$\tau_{conditioning}$ (h)	τ_{mix,H_2O} (h)	$\tau_{conditioning}$ / τ_{mix,H_2O}
Temp = 273 K			
79	3.30E-01	3.64E-03	90.6
53	1.50E+00	2.39E-01	6.3
49	1.50E+00	4.58E-01	3.3
Temp = 283 K			
81	1.60E-01	1.85E-03	86.5
76	1.60E-01	5.00E-03	32.0
55	1.00E+00	2.19E-02	45.7
49	1.00E+00	8.86E-02	11.3
46	1.00E+00	1.94E-01	5.1
42	1.00E+00	4.64E-01	2.2
Temp = 293 K			
90	1.60E-01	1.84E-04	868.3
86	1.60E-01	2.23E-04	718.4
83	1.60E-01	4.18E-04	383.0
79	1.60E-01	7.37E-04	217.2
75	1.60E-01	1.50E-03	106.4

71	1.60E-01	2.03E-03	78.7
50	5.00E-01	1.82E-02	27.5
44	5.00E-01	2.14E-02	23.3
39	5.00E-01	1.48E-01	3.4
34	5.00E-01	5.08E-01	1.0
Temp = 303 K			
73	1.60E-01	8.87E-04	180.5
69	1.60E-01	1.69E-03	94.9
65	1.60E-01	2.65E-03	60.5
50	5.00E-01	6.54E-03	76.5
44	5.00E-01	8.78E-03	56.9
39	5.00E-01	2.69E-02	18.6
34	5.00E-01	5.95E-02	8.4
29	5.00E-01	3.25E-01	1.5

175

176

177

178

References

Evoy, E.: The relationship between diffusion coefficients and viscosity in organic-water matrices as proxies for secondary organic aerosol, The University of British Columbia, 2020.

Evoy, E., Kamal, S., Patey, G. N., Martin, S. T., and Bertram, A. K.: Unified Description of Diffusion Coefficients from Small to Large Molecules in Organic-Water Mixtures, The journal of physical chemistry. A, 124, 2301–2308, 10.1021/acs.jpca.9b11271, 2020.

Evoy, E., Kiland, K. J., Huang, Y., Schnitzler, E. G., Maclean, A. M., Kamal, S., Abbatt, J. P. D., and Bertram, A. K.: Diffusion Coefficients and Mixing Times of Organic Molecules in β-Caryophyllene Secondary Organic Aerosol (SOA) and Biomass Burning Organic Aerosol (BBOA), ACS Earth and Space Chemistry, 5, 3268–3278, 10.1021/acsearthspacechem.1c00317, 2021.

Evoy, E., Maclean, A. M., Rovelli, G., Li, Y., Tsimpidi, A. P., Karydis, V. A., Kamal, S., Lelieveld, J., Shiraiwa, M., Reid, J. P., and Bertram, A. K.: Predictions of diffusion rates of large organic molecules in secondary organic aerosols using the Stokes–Einstein and fractional Stokes–Einstein relations, Atmos. Chem. Phys., 19, 10073–10085, 10.5194/acp-19-10073-2019, 2019.

Grzinic, G., Bartels-Rausch, T., Berkemeier, T., Türler, A., and Ammann, M.: Viscosity controls humidity dependence of N2O5 uptake to citric acid aerosol, Atmospheric Chemistry and Physics, 15, 13615–13625, 10.5194/acp-15-13615-2015, 2015.

Haynes, W. M.: CRC handbook of chemistry and physics, CRC press, 10.1201/9781315380476, 2016.

Hersbach, H., Bell, B., Berrisford, P., Biavati, G., Horányi, A., Muñoz Sabater, J., Nicolas, J., Peubey, C., Radu, R., and Rozum, I.: ERA5 Monthly Averaged Data on Pressure Levels from 1940 to Present., 2023.

Kiland, K. J., Mahrt, F., Peng, L., Nikkho, S., Zaks, J., Crescenzo, G. V., and Bertram, A. K.: Viscosity, glass formation, and mixing times within secondary organic aerosol from biomass burning phenolics, ACS Earth Space Chem., 7, 1388–1400, 10.1021/acsearthspacechem.3c00039, 2023a.

Kiland, K. J., Mahrt, F., Peng, L., Nikkho, S., Zaks, J., Crescenzo, G. V., and Bertram, A. K.: Viscosity, Glass Formation, and Mixing Times within Secondary Organic Aerosol from Biomass Burning Phenolics, ACS Earth and Space Chemistry, 7, 1388–1400, 10.1021/acsearthspacechem.3c00039, 2023b.

Maclean, A. M., Li, Y., Crescenzo, G. V., Smith, N. R., Karydis, V. A., Tsimpidi, A. P., Butenhoff, C. L., Faiola, C., Lelieveld, J., Nizkorodov, S. A., Shiraiwa, M., and Bertram, A. K.: Global Distribution of the Phase State and Mixing Times within Secondary Organic Aerosol Particles in the Troposphere Based on Room-Temperature Viscosity Measurements, ACS Earth and Space Chemistry, 5, 3458–3473, 10.1021/acsearthspacechem.1c00296, 2021.

Petters, M. D. and Kreidenweis, S. M.: A single parameter representation of hygroscopic growth and cloud condensation nucleus activity, Atmos. Chem. Phys., 7, 1961–1971, 10.5194/acp-7-1961-2007, 2007.

Pöschl, U., Martin, S. T., Sinha, B., Chen, Q., Gunthe, S. S., Huffman, J. A., Borrmann, S., Farmer, D. K., Garland, R. M., Helas, G., Jimenez, J. L., King, S. M., Manzi, A. O., Mikhailov, E., Pauliquevis, T., Petters, M. D., Prenni, A. J., Roldin, P., Rose, D., Schneider, J., Su, H., Zorn, S. R., Artaxo, P., and Andreae, M. O.: Rainforest Aerosols as Biogenic Nuclei of Clouds and Precipitation in the Amazon, Science (New York, N.Y.), 329, 1513–1516, 10.1126/science.1191056, 2010.

Price, H. C., Mattsson, J., and Murray, B. J.: Sucrose diffusion in aqueous solution, Physical chemistry chemical physics : PCCP, 18, 19207–19216, 10.1039/c6cp03238a, 2016.

Riipinen, I., Pierce, J. R., Yli-Juuti, T., Nieminen, T., Hakkinen, S. A. K., Ehn, M., Junninen, H., Lehtipalo, K., Petäjä, T., Slowik, J. G., Chang, R. Y. W., Shantz, N., Abbatt, J. P. D., Leaitch, W. R., Kerminen, V. M., Worsnop, D. R., Pandis, S. N., Donahue, N. M., and Kulmala, M.: Organic condensation: a vital link connecting aerosol formation to cloud condensation nuclei (CCN) concentrations, Atmospheric Chemistry and Physics, 11, 3865–3878, 10.5194/acp-11-3865-2011, 2011.

224 Sellier, M., Grayson, J. W., Renbaum-Wolff, L., Song, M., and Bertram, A. K.: Estimating the viscosity of a highly

225 viscous liquid droplet through the relaxation time of a dry spot, Journal of Rheology, 59, 733–750,

226 10.1122/1.4917240, 2015.

227 Smith, N. R., Crescenzo, G. V., Huang, Y., Hettiyadura, A. P., Siemens, K., Li, Y., Faiola, C. L., Laskin, A.,

228 Shiraiwa, M., and Bertram, A. K.: Viscosity and liquid–liquid phase separation in healthy and stressed plant SOA,

229 Environ. Sci.: Atmos., 1, 140–153, 10.1039/D0EA00020E, 2021a.

230 Smith, N. R., Crescenzo, G. V., Huang, Y., Hettiyadura, A. P. S., Siemens, K., Li, Y., Faiola, C., Laskin, A.,

231 Shiraiwa, M., Bertram, A. K., and Nizkorodov, S. A.: Viscosity and liquid–liquid phase separation in healthy and

232 stressed plant SOA, Environmental Science: Atmospheres, 1, 140–153, 10.1039/d0ea00020e, 2021b.

233 Weight, W. D.: Practical Hydrogeology: Principles and Field Applications, McGraw Hill Professional 2019.

234 Winston, P. W. and Bates, D. H.: Saturated Solutions For the Control of Humidity in Biological Research, Ecology,

235 41, 232–237,10.2307/1931961, 1960.

236